

CMB Alignment in Multi-Connected Universes

Ralf Aurich, Sven Lustig, Frank Steiner, and Holger Then¹

Institut für Theoretische Physik, Universität Ulm,
Albert-Einstein-Allee 11, D-89069 Ulm, Germany

Abstract. The low multipoles of the cosmic microwave background (CMB) anisotropy possess some strange properties like the alignment of the quadrupole and the octopole, and the extreme planarity or the extreme sphericity of some multipoles, respectively. In this paper the CMB anisotropy of several multi-connected space forms is investigated with respect to the maximal angular momentum dispersion and the Maxwellian multipole vectors in order to settle the question whether such spaces can explain the low multipole anomalies in the CMB.

PACS numbers: 98.80.-k, 98.70.Vc, 98.80.Es

1. Introduction

The study of the properties of the low multipoles of the cosmic microwave background (CMB) anisotropy requires full-sky maps as provided by the Wilkinson Microwave Anisotropy Probe (WMAP) [1, 2]. These large-scale studies allow to scrutinise the assumptions on statistical isotropy and Gaussianity as predicted by inflationary scenarios. Such an analysis requires a foreground-cleaned map as the Internal Linear Combination (ILC) map [3] and the “TdOH” maps derived by [4]. The best known anomalies at low values of l are the quadrupole suppression and the very small values of the two-point temperature correlation function $C(\vartheta)$ at angular separations $\vartheta \gtrsim 60^\circ$. This low power at angular scales above 60° can be well explained by assuming a multi-connected space for the spatial sections of our Universe. Besides this quadrupole suppression, an anomalous alignment between the quadrupole and the octopole was discovered in [4, 5], the latter being unusually planar. This alignment is described by the axis \hat{n}_l which maximises the *angular momentum dispersion* [4]

$$(\Delta L(\hat{n}))_l^2 := \sum_{m=-l}^l m^2 |a_{lm}(\hat{n})|^2 \quad (1)$$

for a given multipole l . Here $a_{lm}(\hat{n})$ denotes the expansion coefficients of the CMB temperature fluctuation δT with respect to the spherical harmonics $Y_{lm}(\vartheta, \phi)$ with the

¹ Present address: Carl-von-Ossietzky Universität Oldenburg, Institut für Physik, D-26111 Oldenburg, Germany

z -axis pointing in the direction of \hat{n} . This prescription gives for each multipole l only one unit vector \hat{n}_l thus leading to a loss of information.

An alternative statistics with the aim to analyse the multipole alignment is given by [6]

$$r_l := \max_{m,\hat{n}} \frac{\mathcal{C}_{lm}(\hat{n})}{(2l+1)C_l} \quad (2)$$

with $\mathcal{C}_{l0}(\hat{n}) = |a_{l0}(\hat{n})|^2$, $\mathcal{C}_{lm}(\hat{n}) = 2|a_{lm}(\hat{n})|^2$ for $m > 0$ and $(2l+1)C_l = \sum_{m=-l}^l |a_{lm}|^2$. This statistics selects the direction \hat{n} which concentrates the most power into a single m mode. In contrast to (1) the statistics (2) does not prefer the m mode with $m = l$. We find in agreement with [7] that this statistics is very sensitive to noise which changes the selected value of m and in turn leads to a completely different direction \hat{n} . Nevertheless the anomalous multipole alignment is confirmed using (2) in [6].

Instead of the axis \hat{n}_l of maximal angular momentum dispersion (1), one can use multipole vectors [8]. The expansion of a function $f(\vartheta, \phi)$ on the sphere \mathcal{S}^2

$$f(\vartheta, \phi) = \sum_{l=0}^{\infty} f_l(\vartheta, \phi) \quad (3)$$

is provided by the Maxwellian multipole vectors $\hat{v}^{(l,j)}$, $j = 1, \dots, l$, and a scalar $A^{(l)}$ with

$$f_l(\vartheta, \phi) = \left[A^{(l)} (\hat{v}^{(l,1)} \cdot \vec{\nabla}) \cdots (\hat{v}^{(l,l)} \cdot \vec{\nabla}) \frac{1}{r} \right]_{r=1} . \quad (4)$$

The multipole vectors $\hat{v}^{(l,j)}$ together with $A^{(l)}$ contain the complete information about $f(\vartheta, \phi)$ in the same way as the a_{lm} 's of the usual spherical harmonics expansion. For $l = 2$ there is the relation $\hat{n}_2 = \pm \hat{v}^{(2,1)} \times \hat{v}^{(2,2)}$, however for $l > 2$ there does not exist such a simple relation [7].

The multipole vectors have been applied to the CMB anisotropy in [9, 10] in order to study the large-angle anomalies. Area vectors

$$\vec{w}^{(l,i,j)} := \pm \hat{v}^{(l,i)} \times \hat{v}^{(l,j)} \quad (5)$$

are introduced which give the normals to the planes defined by each pair of multipole vectors. The signs are arbitrary and chosen such that the area vectors $\vec{w}^{(l,i,j)}$ point towards the northern galactic hemisphere. The quadrupole plane and the three octopole planes are found to be strongly aligned [10]. Furthermore, three of these four planes are found to be orthogonal to the ecliptic. This result might point to a neglected solar foreground. Correcting this supposed foreground might resolve the mysterious low- l anomalies.

Assuming that there are no unknown foregrounds and no systematic errors in the measurements, the low- l anomalies have to be considered as of cosmological origin. One such possibility is that the statistical isotropy is violated by vorticity and shear contributions in the metric due to a Bianchi VII_h cosmology. Such a model could explain the anomalies but for an unrealistically low value of $\Omega_{\text{tot}} \simeq 0.5$ for a pure matter model [11, 12]. Even the inclusion of dark energy does not lead to more viable cosmological

parameters in order to explain the anomalies [13]. The anomalies could also be caused by matter inhomogeneities of the local Universe ($z \lesssim 1$) as an asymmetric distribution of voids [14] using the usual cosmological parameters, or the quadrupole could be modified by the Local Supercluster via the Sunyaev-Zel'dovich effect [15]. A further possible explanation could be that the quadrupole-octopole alignment is rather an anti-alignment of the quadrupole and the octopole with the dipole. A slightly erroneous treatment of the large dipole could then lead to a spurious quadrupole-octopole alignment [16].

An alternative explanation for the anomalies might come from cosmic topology, where one assumes that the spatial section of the Universe is multi-connected. In [5] toroidal space forms in a flat universe are considered in which one side of the torus has a length below the Hubble radius whereas the other two are above. This so-called slab topology can explain the planarity of the octopole but not the alignment between quadrupole and octopole according to [5]. Based on the vectors \hat{n} determined from the r_l statistics (2), an average alignment angle $\hat{\theta}$ for $l = 2$ to 5 is constructed in [17] and also applied to slab topologies. The very small average alignment angle $\hat{\theta}$ obtained from the TdOH map [4] is improbable in simply-connected spaces. It is claimed [17] that a modest increase in the probability for such a $\hat{\theta}$ value can be obtained for very thin slab spaces. However, as mentioned above, the r_l statistics is very sensitive to noise and, indeed, other full-sky maps possess much larger values of $\hat{\theta}$ as it is the case for the foreground-cleaned maps in the Q, V, and W bands [3] and the ILC map derived from the former, as well as for the “Lagrange-ILC” map of [18]. Thus it may be unnecessary to require very small values of $\hat{\theta}$.

There arises the question what large-angle CMB properties other multi-connected space forms have with respect to the alignment between quadrupole and octopole, and with respect to the multipole vector representation. To that aim we consider in this paper as space manifolds \mathcal{M} three spherical space forms, the toroidal universes in flat space, and the Picard topology in hyperbolic space. The quadrupole-octopole alignment and the multipole vectors corresponding to $l = 2$ and $l = 3$ are investigated for these space forms.

2. The multi-connected space forms

The most remarkable signature of multi-connected universes is a suppression of the CMB power spectrum at large angular scales, in particular a large suppression of the CMB quadrupole and octopole, and of the temperature two-point correlation function at large angles. It is exactly this property which neatly explains the low power at large angles as first observed by COBE [19] and later substantiated by WMAP [1]. For an introduction to “cosmic topology”, see [20, 21].

It is claimed in [22] that the Poincaré dodecahedron (corresponding to the binary icosahedral group I^*) explains well the WMAP data on large scales. Since the CMB computations in [22] are based on very few eigenmodes only, a comparison to the WMAP data using much more eigenmodes is carried out in [23]. Besides the Poincaré

dodecahedron, there are two further good candidates for multi-connected spherical space forms [24] corresponding to the binary tetrahedral group T^* and the binary octahedral group O^* . Spherical topologies based on cyclic groups Z_k or on binary dihedral groups D_{4m}^* do not lead to a sufficient suppression on large scales [25, 24]. Here, we investigate the alignment and multipole vector properties of the binary tetrahedron S^3/T^* , the binary octahedron S^3/O^* , and the Poincaré dodecahedron S^3/I^* .

In flat space there are 17 multi-connected space forms out of which 10 possess a finite volume. From the latter ones we choose the simplest space form, i.e. the hypertorus T^3 , where opposite faces are identified without any rotation. In contrast to space forms of non-flat universes, the size of the space forms in flat universes is independent of the curvature, i.e. of Ω_{tot} and can thus be chosen freely. Below, the side lengths L of the hypertori will be given in units of the Hubble radius $a_0 = \frac{c}{H_0}$. For the selected cosmological parameters the radius of the surface of last scattering (SLS) is $\eta_{\text{SLS}} = 3.267$.

The above described space forms are homogeneous. An example of a non-homogeneous space form is the Picard topology of hyperbolic space. This model is discussed in the framework of cosmology in [26, 27]. Although its fundamental cell possesses an infinitely long horn, and is thus non-compact, it has a finite volume. The shape of the fundamental cell is that of a hyperbolic pyramid with one cusp at infinity, see [26] for details. Because of its inhomogeneity, the considered statistics depends on the position of the observer. In the following we choose two positions, one “near” to the cusp and the other “far away” from it. For definiteness, choosing the upper half-space as the model of hyperbolic space with Gaussian curvature $K = -1$, the two observers A and B are at $(x_1, x_2, x_3) = (0.2, 0.1, 1.6)$ and $(0.2, 0.1, 5.0)$, respectively [26].

This non-compact space form has the special property that the spectrum corresponding to the Laplace-Beltrami operator is not purely discrete; instead its discrete spectrum is imbedded in a continuous spectrum. The eigenfunctions of the discrete spectrum are the Maaß cusp forms and those of the continuous spectrum are given by an Eisenstein series. The two types of eigenfunctions have different properties and are discussed separately in the following.

3. The quadrupole-octopole alignment

The angular momentum dispersion (1) leads for each multipole l to one unit vector \hat{n}_l as discussed in the Introduction. The quadrupole-octopole alignment was revealed in [4, 5] by considering the dot product

$$A_{23} := |\hat{n}_2 \cdot \hat{n}_3| . \quad (6)$$

For the TdOH sky map the surprisingly high value of $A_{23} \simeq 0.9849$ [5] was found corresponding to an angular separation between \hat{n}_2 and \hat{n}_3 of only 10° . This result is essentially confirmed using the WMAP 3yr measurements independent of the used mask to eliminate galactic foregrounds [28]. Under the assumption that the CMB is an isotropic random field, all multipoles are statistically independent and all directions of

the \hat{n}_l 's are equally probable. In this case the values of A_{23} are *uniformly* distributed on the interval $[0, 1]$. A value greater than $A_{23} = 0.9849$ is thus obtained only for 1.51% of isotropic CMB realizations.

The root of the quadrupole-octopole alignment is the unusual behaviour of the a_{lm} 's for $l = 2$ and $l = 3$. They have the property that there exists a coordinate system in which all values of $|a_{lm}|$ are very small except $|a_{ll}|$ and $|a_{l0}|$ (see Table III in [5]). Since the value of $|a_{l0}|$ is irrelevant for the angular momentum dispersion (1), the alignment points to models of the universe having small values of $|a_{lm}|/|a_{ll}|$ for $m = 1, \dots, l-1$. Two conditions are necessary for this to be the case:

- i) The lowest eigenfunctions of the multi-connected space \mathcal{M} should possess spherical expansion coefficients $a_{lm}(n, i)$ which satisfy the topological alignment condition

$$\frac{|a_{lm}(n, i)|}{|a_{ll}(n, i)|} \ll 1 \quad \text{for } m = 1, \dots, l-1 \quad \text{and } l = 2, 3 \quad .$$

Here n counts the eigenvalues and i is the degeneracy index $i = 1, \dots, r^{\mathcal{M}}(n)$, where $r^{\mathcal{M}}(n)$ is the multiplicity of the n th eigenvalue.

- ii) The transfer function $T_l(k)$ [29] should emphasize those lowest eigenfunctions with wave-number $k = k_n$ which have the property i) and suppress all others.

One has to enforce condition i) for the lowest eigenfunctions because they give the most important contribution to the CMB fluctuations at large scales and because the separation between consecutive eigenmodes is most pronounced in the lower part of the spectrum. Property i) is so unusual that only a few eigenmodes will possess it. At the higher part of the spectrum the eigenmodes are lying so close together that the transfer functions and the random expansion coefficients will statistically destroy the alignment.

Whereas property i) is determined by the multi-connected space form, property ii) is determined by the cosmological parameters. In the flat case one has, in addition, the freedom to scale the size of the space form instead of the cosmological parameters. Thus it does not suffice to have a manifold with alignment, one also needs cosmological parameters leading to a transfer function which enables the survival of the alignment in the CMB fluctuations.

3.1. The flat hypertorus

Let us demonstrate this dependence on the transfer function in the case of the flat hypertorus, where all three sides are chosen to be equal. The fundamental cell is thus a cube and the lowest eigenvalue is sixfold degenerate. All six eigenfunctions are surprisingly close to our property i). Let us define the *topological alignment measure* $b_{lm}(n)$ as the following sum over all eigenfunctions belonging to the n th-eigenvalue k_n^2

$$b_{lm}(n) := \sum_{i=1}^{r^{\mathcal{M}}(n)} |a_{lm}(n, i)|^2 = \sum_{i=1}^{r^{\mathcal{M}}(n)} \left| Y_{lm} \left(\frac{\vec{k}_i}{|\vec{k}_i|} \right) \right|^2 \quad , \quad (7)$$

where $a_{lm}(n, i)$ is the spherical expansion coefficient of the eigenfunction belonging to the wavevectors \vec{k}_i with $i = 1, \dots, r^M(n)$. To obtain from (7) a unique quantity, one has to choose the value of equation (7) for that rotated coordinate system for which the property i) is optimally satisfied. Figure 1 shows that the hypertorus with equal side lengths has ground state eigenfunctions with are nearly optimal. For $l = 2$ all six eigenfunctions possess $a_{21}(1, i) = 0$ and thus, $b_{21}(1) = 0$ is obtained. In the case $l = 3$ the measure $b_{32}(1)$ vanishes, but $b_{31}(1)$ is not zero. Would the latter also be zero, the first six eigenfunctions belonging to the first eigenvalue would all have the optimal topological alignment. Figure 1 reveals that the next eigenvalues do not possess such a nice alignment behaviour, although there are some special cases like $b_{21}(4)$ or $b_{32}(4)$, which vanish as in the case $n = 1$.

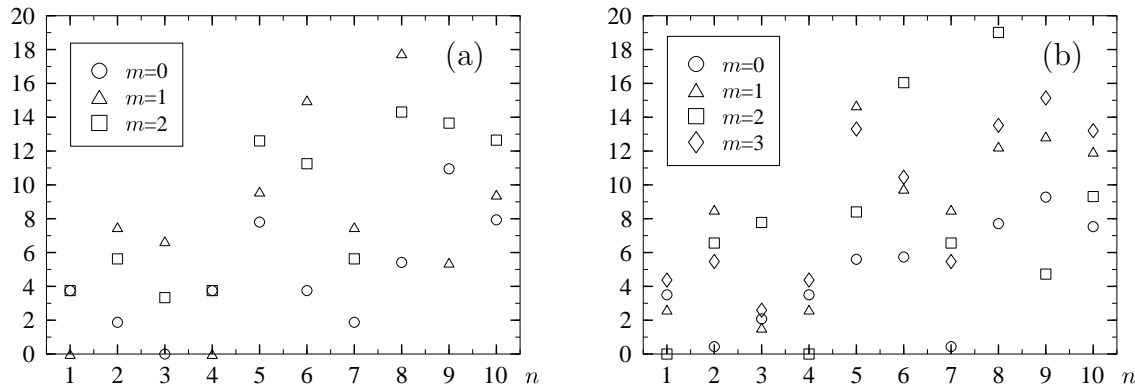


Figure 1. The topological alignment measure (7) is shown for the hypertorus. Panel (a) shows the values of $b_{lm}(n)$ for $l = 2$ for the first ten eigenvalues. Panel (b) displays the analogous quantities for $l = 3$.

This is the point where the transfer function $T_l(k)$ becomes important. According to our property ii) one needs a transfer function, which emphasizes exactly those eigenvalues having a maximal topological alignment. In our example a transfer function $T_l(k)$ which is large for $l = 2$ and $l = 3$ at $n = 1$ and $n = 4$ and small at $n = 2, 3, 5$ would produce more aligned CMB sky maps than a model with a simply-connected space form. In figure 2 the transfer function $T_l(k)$ is shown for the cosmological parameters $\Omega_{\text{bar}} = 0.046$, $\Omega_{\text{cdm}} = 0.234$, $\Omega_{\Lambda} = 0.72$, and $h = 0.7$. Here, reionization is omitted having only a modest influence on such large scales like $l = 2$ and $l = 3$, and a standard thermal history of the neutrinos is assumed. The side length L of the cube determines the scaling of the eigenvalue spectrum. Panel (a) of figure 2 shows the transfer function $T_l(k)$ for a hypertorus with $L = 1.0$, whereas in panel (b) $L = 2.0$ is chosen. One observes in figure 2 that for $L = 1.0$ the first eigenvalue is emphasized by $T_l(k_n)$ for $l = 2$ and $l = 3$. For $L = 2.0$ the opposite behaviour is revealed, i. e. the contribution of the first six eigenfunctions belonging to the first eigenvalue is suppressed. Thus, one expects varying deviations from the uniform distribution for A_{23} , eq. (6), depending on the side length L .

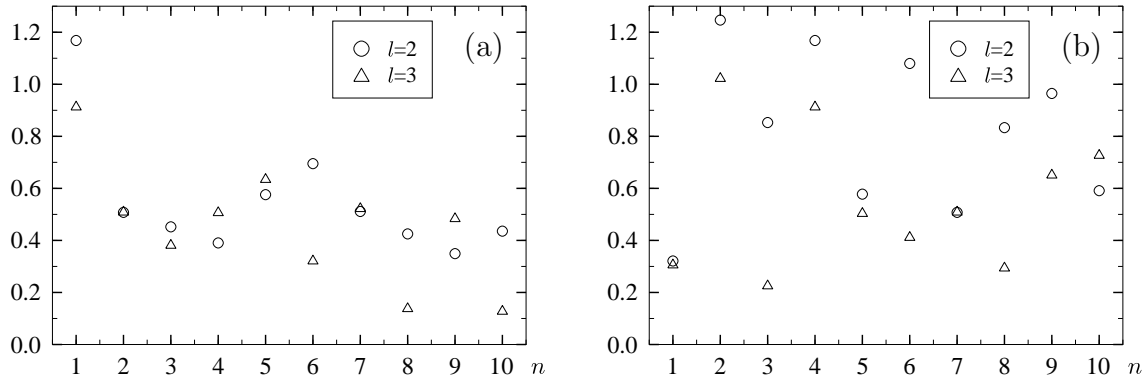


Figure 2. The transfer function $T_l(k_n)$ is shown for a hypertorus with side length $L = 1.0$ (a) and with $L = 2.0$ (b). The abscissae give the number of the eigenvalue n instead of the eigenvalue k_n .

Now we discuss the value distribution of A_{23} for the hypertorus in dependence on the side length L . For each given cube specified by L we generate 100 000 sky realizations with a wave number cut-off $k = 60$ in units of the Hubble length. This allows an accurate determination of the maximum angular momentum dispersion vectors \hat{n}_2 and \hat{n}_3 in order to compute A_{23} . The results for the flat hypertorus are shown in figure 3. In panel (a) the cumulative distribution is shown for 100 000 realizations for a torus with side length $L = 1.0$ together with the uniform distribution. The cumulative distribution for $L = 2.0$ would be indistinguishable from the uniform distribution in this figure. Thus panel (b) displays the difference to the uniform distributions for $L = 1.0$ and $L = 2.0$. As expected from the above discussion, the case $L = 1.0$ where the transfer function $T_l(k_n)$ enhances the contribution of the first eigenvalue displays large deviations from the uniform distribution, whereas in the other case, the obtained distribution is nearly uniform. This demonstrates that one not only needs a space form with “aligned” eigenfunctions but also suitable cosmological parameters.

To address the question whether the deviations are significant, the Kolmogorov-Smirnov test is applied to the distribution of A_{23} with respect to the uniform distribution. This test gives the probability P_{KS} that the maximal deviation Δ from an assumed distribution is in accordance with Gaussian fluctuations given a finite set of N data points. The maximal deviation Δ is shown for a large sequence of side lengths L in figure 4. For each side length L denoted by a small circle, $N = 100 000$ simulations have been carried out. One recognises the large deviation at the side length $L = 1.0$ as already discussed above as well as only a small deviation in the case $L = 2.0$. Once again, the importance of the transfer function $T_l(k_n)$ is obvious since all eigenfunctions possess the same topological alignment $b_{lm}(n)$ as seen in figure 1. In figure 5 the Kolmogorov-Smirnov probability P_{KS} is displayed with respect to the $N = 100 000$ simulations. The horizontal line lies at a probability of 5%. Hypertori below this significance level can be considered as having a too large maximal deviation Δ to be compatible with statistical fluctuations. These are the hypertori whose values of A_{23} are not uniformly distributed.

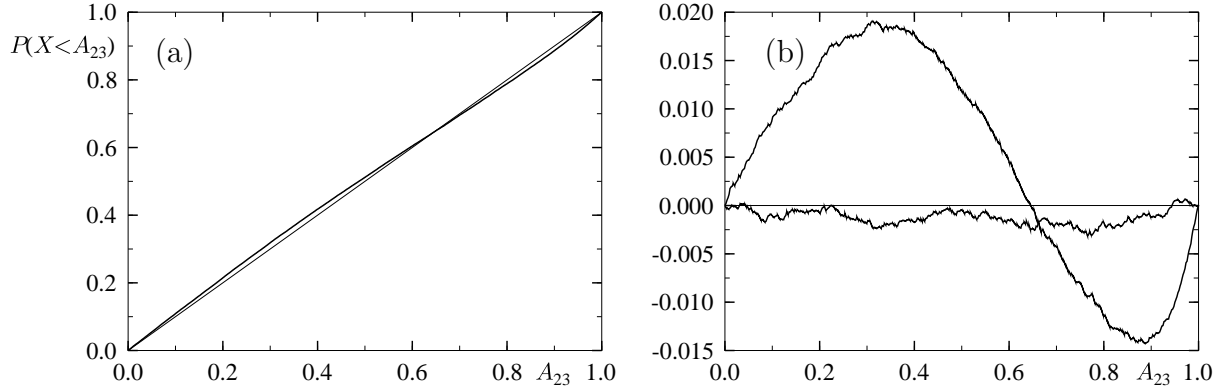


Figure 3. The cumulative distribution $P(X < A_{23})$ is shown for the hypertorus with side length $L = 1.0$ together with the uniform distribution (straight line) in panel (a). Since the curve for $L = 2.0$ would be indistinguishable from the uniform distribution, panel (b) shows the difference to the uniform distribution for the torus with side length $L = 1.0$ (large deviations from the zero line) and with side length $L = 2.0$ (small deviations), respectively.

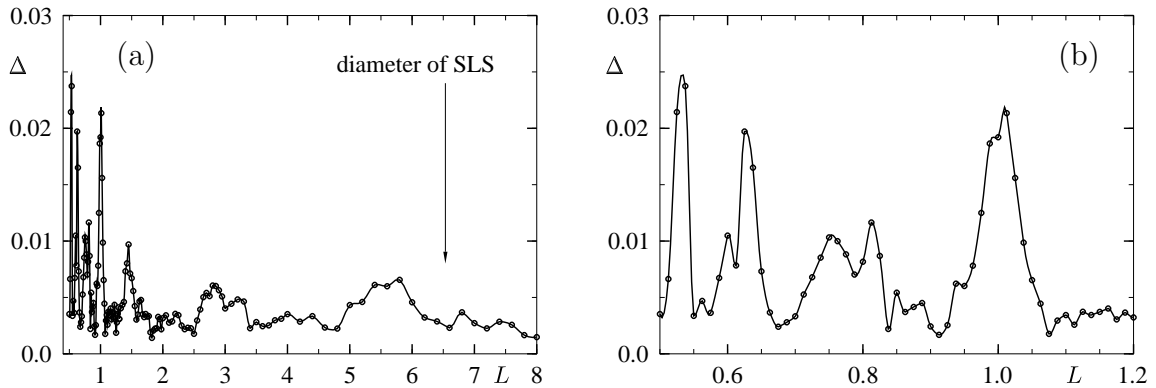


Figure 4. The maximal deviation Δ of the cumulative distribution $P(X < A_{23})$ from the uniform distribution is shown in dependence of the side length L of the hypertori. The diameter of the SLS at $2\eta_{\text{SLS}} = 6.534$ is indicated. Models with a side length L below this value are completely within the SLS.

The observed value of A_{23} very close to one can hardly be explained by the flat hypertori. A value greater than the observed one of $A_{23} = 0.9849$ is obtained only for 1.51% of isotropic CMB realizations. In figure 6 this value is compared with our sequence of tori. For those tori where the Kolmogorov-Smirnov test signals significant deviation from the uniform expectation, one observes indeed a higher percentile up to roughly 2% of models having larger values than $A_{23} = 0.9849$. One gets for these model an increased probability for the alignment but it is a matter of personal judgement whether one considers a 1:50 probability as a serious problem.

Let us now demonstrate how difficult it is to obtain such a strong alignment as it is observed in the CMB sky. To that aim we return to the cube with side length $L = 1.0$ which already possesses a statistically significant deviation from the uniform distribution. We now artificially alter some expansion coefficients to increase

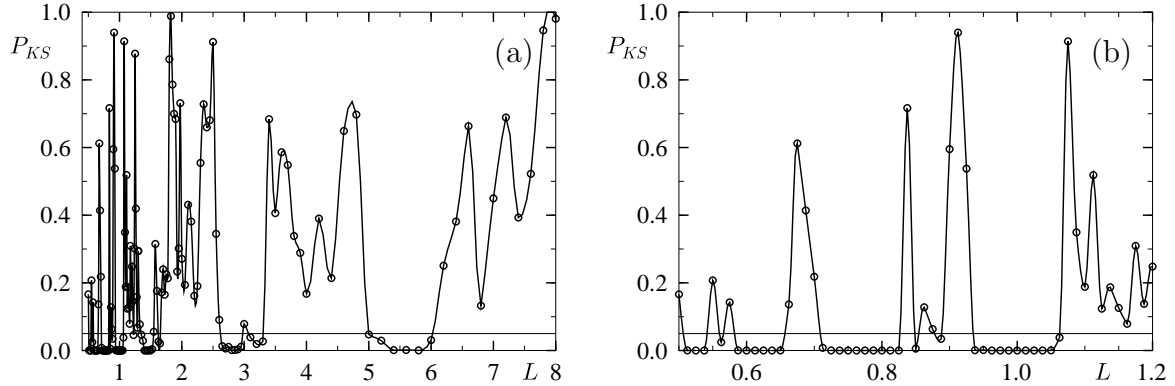


Figure 5. The Kolmogorov-Smirnov test is applied to the distribution of the values of A_{23} compared to the uniform distribution for hypertori with side lengths L covering the interval $L \in [0.5, 8]$.

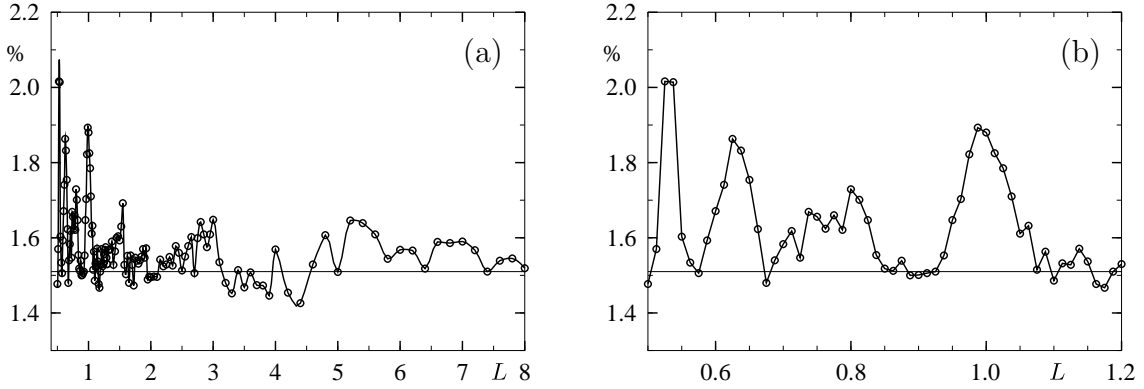


Figure 6. The percentile of the models having a larger value of A_{23} than the observed value of $A_{23} = 0.9849$ is shown. For a uniform distribution one expects a percentile of 1.51% which is indicated by the horizontal line.

the topological alignment or alter the transfer function to enhance the contribution of the first eigenvalue. At first we show that the deviation is indeed due to the contribution belonging to the first eigenvalue. In figure 7a the distribution of A_{23} is compared with one where the contribution of the six eigenfunctions belonging to the first eigenvalue is artificially omitted. This omission leads indeed to a equidistribution as seen in figure 7a. Whereas 1.880% of the hypertorus models with $L = 1.0$ have a larger value of A_{23} than the observed value of $A_{23} = 0.9849$, there are only 1.518% of models with the omitted ground state. In figure 7b we alter the spherical expansion coefficients a_{31} by multiplying them by 0.001 for $n = 1$. This leads for the first eigenvalue to a nearly perfect topological alignment. However, this does not change the histogram significantly showing that the next eigenvalues are important too and destroy the alignment provided by the first eigenvalue. The percentile of such models with $A_{23} > 0.9849$ is 1.770%. In the next step we multiply again a_{31} by 0.001 for $n = 1$, but, in addition, we omit the contributions of the second to the tenth eigenvalue producing artificially a large gap in the eigenvalue spectrum. This leads to the distribution shown in figure 7c possessing a

large “alignment peak” at $A_{23} = 1$. Further increasing the gap artificially makes this peak more pronounced as shown in 7d where the contributions of the eigenvalues from $n = 2$ to $n = 30$ are omitted. The corresponding percentiles for $A_{23} > 0.9849$ are 3.627% and 9.103%, respectively.

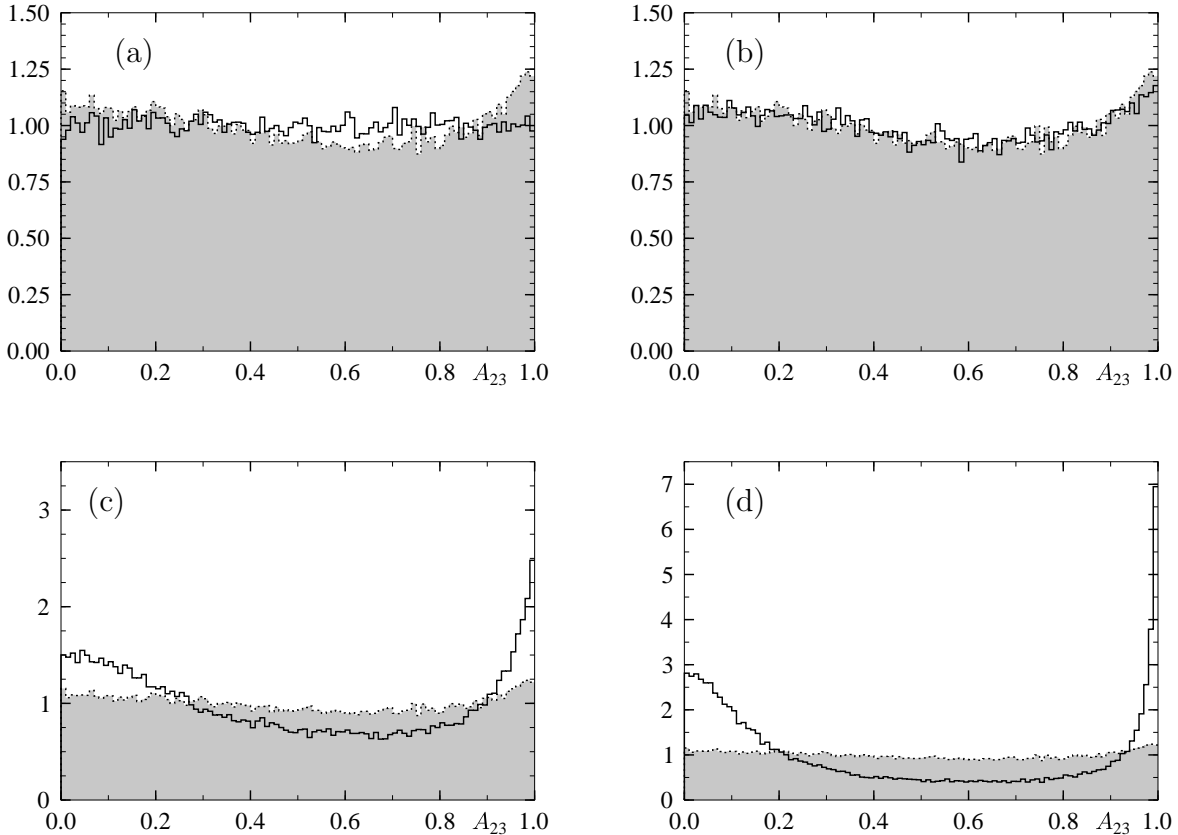


Figure 7. The distribution of A_{23} for the hypertorus with side length $L = 1.0$ is shown as a dotted curve in all four panels. As a full curve modified computations are shown: in panel (a) the contribution of the first eigenvalue $n = 1$ is omitted, in panel (b) the expansion coefficient a_{31} is multiplied by 0.001 for the eigenfunctions belonging to the first eigenvalue, and in addition to this multiplication, in panels (c) and (d) the contribution of the eigenvalues $n = 2, \dots, 10$ and $n = 2, \dots, 30$ are omitted, respectively.

In order to find a space form possessing a strong alignment A_{23} , two requirements are important. On the one hand a space form is needed where the eigenfunctions of the first eigenvalue possess a strong topological alignment, property i), and on the other hand, the gap between the first eigenvalue and the second should be as large as possible such that the required property ii) can lead to a survival of the topological alignment of the first eigenfunctions.

Slab topologies are considered with respect to the average alignment angle $\hat{\theta}$ in [17]. There it is found that the average alignment angle $\hat{\theta}$ deviates from the uniform expectation the more the thinner the fundamental cells are. It is an interesting question whether this behaviour is really monotone or whether a higher resolution with respect

Table 1. The maximal deviation Δ from the uniform distribution and the corresponding Kolmogorov-Smirnov probability P_{KS} are shown for three spherical spaces for three sets of cosmological parameters. The values are based on 100 000 CMB sky map realizations for each model.

spherical model	Δ	P_{KS}	$P(A_{23} > 0.9849)$
\mathcal{S}^3/T^* , $\Omega_{\text{tot}} = 1.018$	0.00717	0.0%	1.481%
\mathcal{S}^3/T^* , $\Omega_{\text{tot}} = 1.038$	0.05015	0.0%	1.147%
\mathcal{S}^3/T^* , $\Omega_{\text{tot}} = 1.065$	0.01672	0.0%	1.423%
\mathcal{S}^3/O^* , $\Omega_{\text{tot}} = 1.018$	0.03107	0.0%	1.246%
\mathcal{S}^3/O^* , $\Omega_{\text{tot}} = 1.038$	0.00952	0.0%	1.376%
\mathcal{S}^3/O^* , $\Omega_{\text{tot}} = 1.065$	0.01836	0.0%	1.397%
\mathcal{S}^3/I^* , $\Omega_{\text{tot}} = 1.018$	0.00347	18.0%	1.527%
\mathcal{S}^3/I^* , $\Omega_{\text{tot}} = 1.038$	0.00237	62.8%	1.552%
\mathcal{S}^3/I^* , $\Omega_{\text{tot}} = 1.065$	0.00222	70.7%	1.488%

to the thickness of the slabs also reveals a fluctuating behaviour dictated by the transfer function.

3.2. Three models with positive spatial curvature

Let us now discuss the alignment properties of the three spherical space forms \mathcal{S}^3/T^* , \mathcal{S}^3/O^* , and \mathcal{S}^3/I^* [24]. Because it requires a large numerical effort to simulate and analyse a huge number of sky maps, we do not analyse the parameter space so extensively as in the case of the hypertorus. Instead we choose the three different sets of cosmological parameters for which these three models give a satisfactory description of the large-scale CMB anisotropy [24]. The cosmological parameters are $\Omega_{\text{bar}} = 0.046$, $\Omega_{\text{cdm}} = 0.234$, and $h = 0.7$. The dark energy contribution varies as $\Omega_{\Lambda} = 0.738$, $\Omega_{\Lambda} = 0.758$, and $\Omega_{\Lambda} = 0.785$, which leads to $\Omega_{\text{tot}} = 1.018$, $\Omega_{\text{tot}} = 1.038$, and $\Omega_{\text{tot}} = 1.065$, respectively. These three different values of Ω_{tot} lead to different sizes of the fundamental cells. The cells are the larger the closer Ω_{tot} is to one. E.g. for the Poincaré dodecahedron \mathcal{S}^3/I^* , the surface of last scattering fits completely inside the fundamental cell below $\Omega_{\text{tot}} \simeq 1.01$. In that case no circles-in-the-sky signature can be observed.

The results are shown in table 1 and in figures 8 to 10. The eigenfunctions of the Poincaré dodecahedron \mathcal{S}^3/I^* do not fulfil the property i). Although it possesses a large gap in the eigenvalue spectrum between $n = 1$ and $n = 2$, which would facilitate to satisfy property ii), the sky maps are without property i) not aligned for this space form as inferred from table 1 and figure 10. This is in contrast to the other two spherical space forms, i. e. \mathcal{S}^3/T^* and \mathcal{S}^3/O^* . Here the deviations are so large such that the Kolmogorov-Smirnov test yields almost zero probabilities P_{KS} . However, these two space forms possess an anti-alignment leading to a smaller probability for $P(A_{23} > 0.9849)$ than a uniform distribution, see table 1. Thus, these spherical space forms cannot explain the

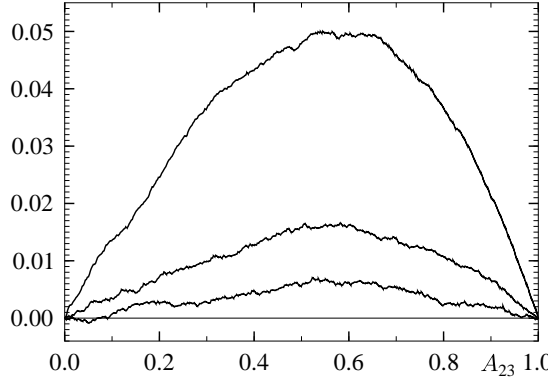


Figure 8. The deviation of the cumulative distribution $P(X < A_{23})$ from the uniform distribution is shown for the binary tetrahedron S^3/T^* for $\Omega_{\text{tot}} = 1.018, 1.038$, and 1.065 .

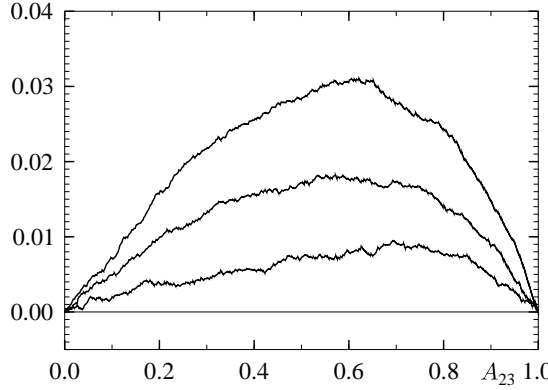


Figure 9. The deviation of the cumulative distribution $P(X < A_{23})$ from the uniform distribution is shown for the binary octahedron S^3/O^* for $\Omega_{\text{tot}} = 1.018, 1.038$, and 1.065 .

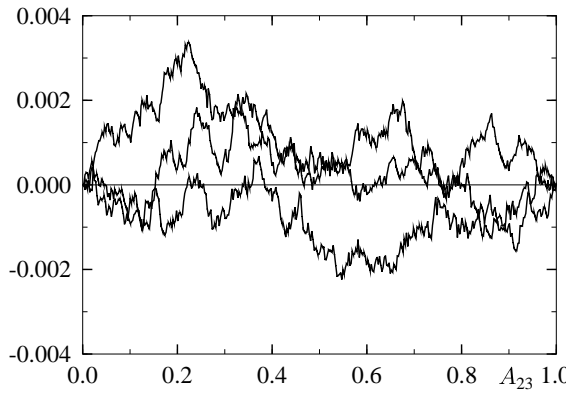


Figure 10. The deviation of the cumulative distribution $P(X < A_{23})$ from the uniform distribution is shown for the Poincaré dodecahedron S^3/I^* for $\Omega_{\text{tot}} = 1.018, 1.038$, and 1.065 .

quadrupole-octopole alignment as a topological effect.

3.3. An inhomogeneous model with negative spatial curvature

In the case of the hyperbolic Picard topology [26, 27] we show the cumulative distribution $P(X < A_{23})$ for a nearly flat model with $\Omega_{\text{tot}} = 0.95$ ($\Omega_m = \Omega_{\text{bar}} + \Omega_{\text{cdm}} = 0.3$, $\Omega_\Lambda = 0.65$, and $h = 0.7$). Because of the larger deviations from the uniform distribution, $P(X < A_{23})$ is shown in figure 11. The Kolmogorov-Smirnov test gives almost zero probabilities P_{KS} compared to the uniform distribution. Thus, this inhomogeneous space form clearly shows a non-uniform distribution of A_{23} in contrast to the homogeneous space forms considered before. One obtains 1.692%, 3.818%, 1.768%, and 8.856% out of 100 000 realizations possessing values of A_{23} larger than $A_{23} = 0.9849$ for the observer A far away from the horn using either the cusp modes or the Eisenstein modes, and for the observer B in the horn using again either cusp or Eisenstein modes, respectively. Thus, while the cusp modes yield a small correlation between the quadrupole and the octopole, the Eisenstein modes display a clear tendency for a quadrupole-octopole alignment. However, as discussed in [26], the primordial curvature perturbations are composed of both the cusp and the Eisenstein modes. Because of their different nature, the former belonging to the discrete spectrum and being square integrable and the latter belonging to the continuum being normalizable only to a Dirac- δ distribution, there is no hint of their relative contribution to the primordial perturbations. A superposition of both types of modes would thus diminish the alignment effect of the Eisenstein modes. However, one has found here a topological space form which has naturally a higher quadrupole-octopole alignment.

4. Multipole vectors in multi-connected spaces

The large-scale CMB anomalies have also been studied with respect to the Maxwell multipole vectors for the low multipoles. Let us introduce the corresponding quantities for which we will present the statistical properties for multi-connected space forms. From the area vectors (5) the following scalar products can be formed [10] for $l = 2$ and $l = 3$

$$\begin{aligned}\tilde{A}_1 &= |\vec{w}^{(2,1,2)} \cdot \vec{w}^{(3,1,2)}| \\ \tilde{A}_2 &= |\vec{w}^{(2,1,2)} \cdot \vec{w}^{(3,1,3)}| \\ \tilde{A}_3 &= |\vec{w}^{(2,1,2)} \cdot \vec{w}^{(3,2,3)}| .\end{aligned}\tag{8}$$

Ordered with respect to their magnitudes, the scalar products are denoted by A_1 , A_2 and A_3 , i. e. $A_1 > A_2 > A_3$. The analogous scalar products D_1 , D_2 and D_3 are obtained by using normalised vectors $\vec{w}^{(l,i,j)} / |\vec{w}^{(l,i,j)}|$ instead of the area vectors $\vec{w}^{(l,i,j)}$ in (8). From these dot products the following statistical measures can be constructed

$$S_m := \frac{1}{m} \sum_{i=1}^m A_i , \quad m = 1, 2, 3\tag{9}$$

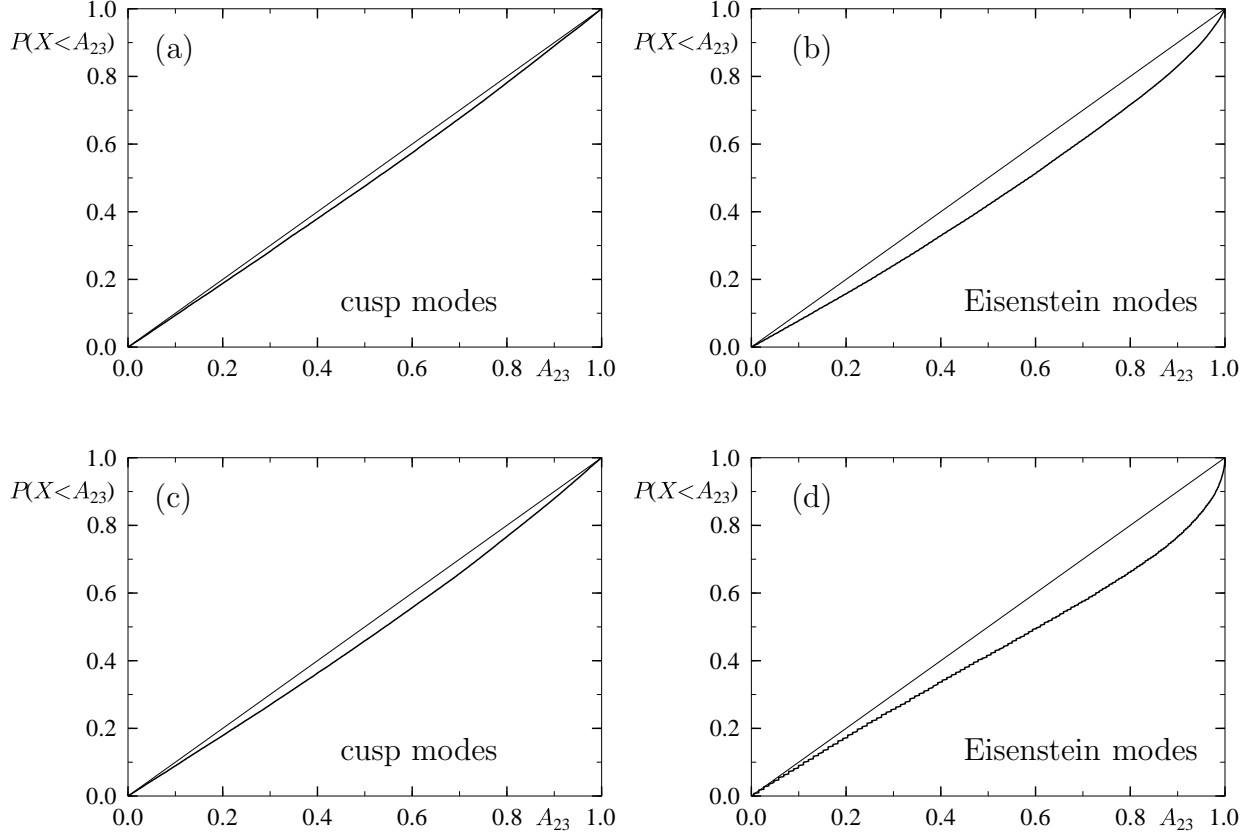


Figure 11. The cumulative distribution $P(X < A_{23})$ is shown for 100 000 realizations of the Picard space with $\Omega_m = \Omega_{\text{bar}} + \Omega_{\text{cdm}} = 0.3$ and $\Omega_\Lambda = 0.65$. Panels (a) and (b) show the results for the “lower” observer point, whereas in panels (c) and (d) the observer point is high up in the horn.

and

$$T_m := 1 - \frac{1}{m} \sum_{i=1}^m (1 - A_i)^2 \quad , \quad m = 1, 2, 3 \quad . \quad (10)$$

There are several estimates for A_i and D_i obtained from the WMAP observations based on the different maps derived from the data [7, 30]. The change of the quadrupole in the ILC 3yr map (see e.g. fig. 7 in [28]) has caused slightly different values in the 3 year data [30] but all give surprisingly high values. In figure 12 we show the corresponding values as vertical lines obtained from the TdOH map [4]

$$A_1 = 0.851 \quad , \quad A_2 = 0.783 \quad , \quad A_3 = 0.762 \quad , \quad (11)$$

and

$$D_1 = 0.953 \quad , \quad D_2 = 0.872 \quad , \quad D_3 = 0.838 \quad . \quad (12)$$

From these values the values for S_m and T_m follow by (9) and (10). The alignment causes large values for A_i , D_i , S_m , and T_m for $i, m = 3$, which are untypical for a “generic” sky map. In figure 12 the distributions for these quantities are shown obtained from 10^5

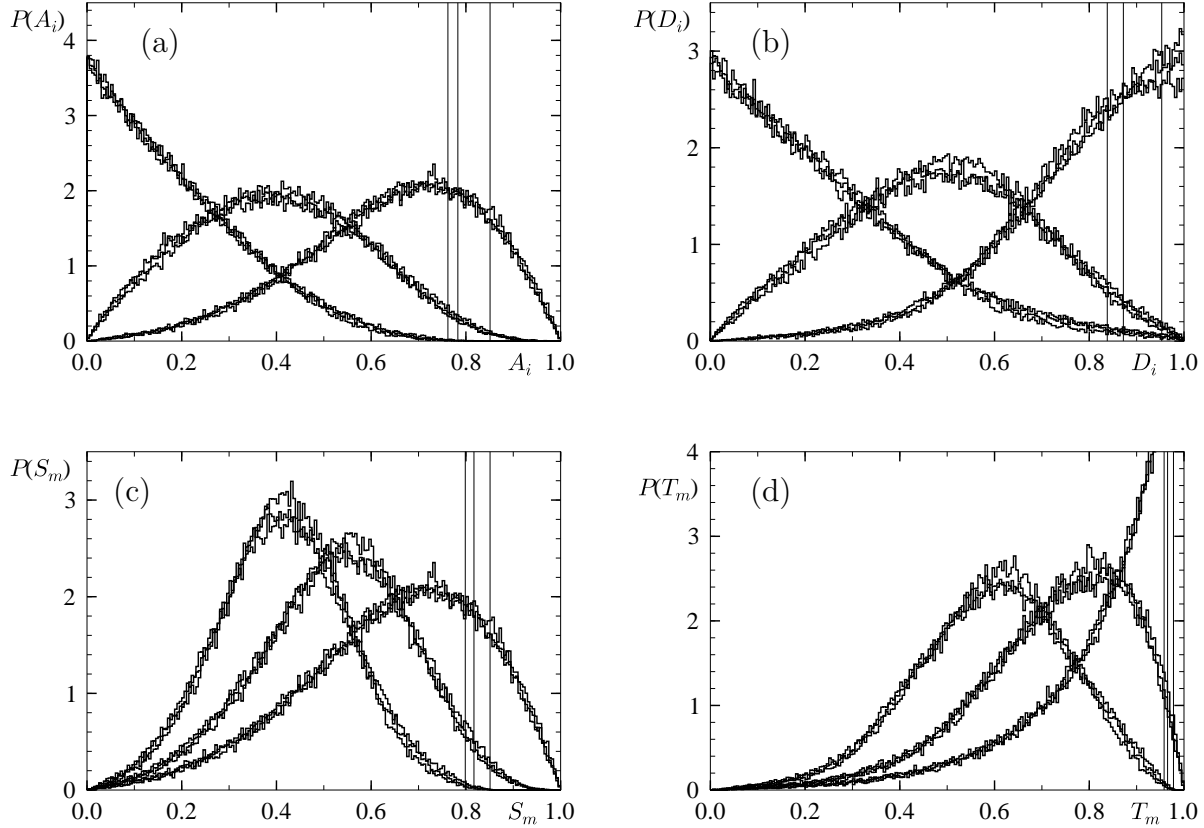


Figure 12. The distributions of A_i (panel a), D_i (panel b), S_m (panel c), and T_m (panel d) with $i, m = 1, 2, 3$ are presented for the torus with side length $L = 1.0$, the dodecahedron \mathcal{S}^3/I^* for $\Omega_{\text{tot}} = 1.018$, and the Picard topology using the cusp modes for the observer position A . The histograms are based on 10^5 sky realizations. The vertical lines indicate the corresponding WMAP values obtained from the TdOH sky map.

sky realizations for the following three topological spaces: the torus with side length $L = 1.0$, the dodecahedral space \mathcal{S}^3/I^* with $\Omega_{\text{tot}} = 1.018$, and the Picard topology using the cusp modes for the observer position A for $\Omega_{\text{tot}} = 0.95$. All models are plotted onto the same corresponding graph since they give very similar distributions which are in turn similar to simply-connected space forms.

In panel (a) the distributions for A_i , $i = 1, 2, 3$ are shown. With increasing value of i , the maxima of the histograms shift to smaller values, of course. The observed WMAP value for A_1 is not unusual as a comparison with the corresponding histograms reveals. The value of A_3 , however, has only a marginal overlap with the tail of the corresponding histograms for all three considered topologies. The same behaviour is observed for the normalized scalar products D_i shown in panel (b). In [31] the distribution of D_i is studied simultaneously for $i = 1, 2, 3$ for the dodecahedral space \mathcal{S}^3/I^* and found to be equidistributed, i. e. if all three histograms in our panel (b) would be added. This is in agreement with our results. We applied the Kolmogorov-Smirnov test which shows for the dodecahedral space \mathcal{S}^3/I^* an equidistribution. The other two spherical space forms

yield zero probabilities for that in agreement with the above results.

In panels (c) and (d) the distributions for S_m and T_m , eqs. (9) and (10), are shown. Again the distributions with smaller values at their maxima belong to higher values of m . As it is the case for A_3 and D_3 , there is only a very small overlap with the tail of the distributions for S_3 and T_3 with the corresponding observed values.

Since the four distributions are similar for the simply-connected universes and the considered multi-connected space forms, the non-trivial topology does not help to explain the anomalous quadrupole and octopole properties. But that does not disfavour multi-connected space forms, since the simply-connected alternatives do not yield higher probabilities to remedy the anomalous behaviour. As discussed in the introduction there are several suggestions that the anomalous quadrupole and octopole properties are not of cosmological origin. In that case no explanation would be required from a satisfactory cosmological concordance model.

5. Conclusion

We have investigated the question whether the strange alignment observed in low CMB multipoles can be explained by multi-connected space forms. There are several examples of such spaces which can explain the missing anisotropy power at large angular scales as measured by the temperature correlation function $C(\vartheta)$, $\vartheta > 60^\circ$, or the angular power spectrum C_l for $l = 2, 3$. It is thus natural to ask for the alignment properties in such spaces.

It is shown that two requirements are necessary for a non-trivial topology to be able to generate the observed alignment. The eigenfunctions belonging to the smallest eigenvalue have to obey a strong topological alignment, i. e. they should already have an aligned quadrupole and octopole. In order to make the survival of this property possible in CMB sky maps, it is necessary that the transfer function $T_l(k)$ gives those eigenfunctions with a topological alignment a sufficiently strong weight. In the case of the hypertorus we demonstrate this connection explicitly. It is found that depending on the chosen side length of the hypertorus the CMB sky maps are slightly aligned in some cases and in others not. The alignment is, however, not strong enough in order to state that the hypertorus model could solve the alignment riddle. In addition, three spherical models are considered of which one, the dodecahedron, shows no alignment whereas the other two, the binary tetrahedron and the binary octahedron, display anti-alignment which reduces the probability in comparison to isotropic models. Furthermore, as an example of an inhomogeneous space form, the Picard model of hyperbolic space is studied. This model provides an example of a space form possessing an intrinsic alignment which increases the probability compared to isotropic models.

But in no case we have found a model, where a significant fraction of the simulations possesses the alignment observed in the CMB sky. It remains to be seen whether there are other space forms which can more easily explain the alignment than the space forms considered in this paper.

Acknowledgment

The computation of the multipole vectors $\hat{v}^{(l,j)}$ has been carried out with the algorithm kindly provided by [9].

References

- [1] C. L. Bennett *et al.*, *Astrophys. J. Supp.* **148**, 1 (2003), astro-ph/0302207.
- [2] G. Hinshaw *et al.*, (2006), astro-ph/0603451.
- [3] C. L. Bennett *et al.*, *Astrophys. J. Supp.* **148**, 97 (2003), astro-ph/0302208.
- [4] M. Tegmark, A. de Oliveira-Costa, and A. J. S. Hamilton, *Phys. Rev. D* **68**, 123523 (2003), astro-ph/0302496.
- [5] A. de Oliveira-Costa, M. Tegmark, M. Zaldarriaga, and A. Hamilton, *Phys. Rev. D* **69**, 063516 (2004), astro-ph/0307282.
- [6] K. Land and J. Magueijo, *Phys. Rev. Lett.* **95**, 071301 (2005).
- [7] C. J. Copi, D. Huterer, D. J. Schwarz, and G. D. Starkman, *Mon. Not. R. Astron. Soc.* **367**, 79 (2006), astro-ph/0508047.
- [8] J. C. Maxwell, *A Treatise on Electricity and Magnetism* (Clarendon Press, London, 1891), Vol. I.
- [9] C. J. Copi, D. Huterer, and G. D. Starkman, *Phys. Rev. D* **70**, 043515 (2004), astro-ph/0310511.
- [10] D. J. Schwarz, G. D. Starkman, D. Huterer, and C. J. Copi, *Phys. Rev. Lett.* **93**, 221301 (2004), astro-ph/0403353.
- [11] T. R. Jaffe, A. J. Banday, H. K. Eriksen, K. M. Górska, and F. K. Hansen, *Astrophys. J. Lett.* **629**, L1 (2005).
- [12] K. Land and J. Magueijo, *Mon. Not. R. Astron. Soc.* **367**, 1714 (2006), astro-ph/0509752.
- [13] T. R. Jaffe, S. Hervik, A. J. Banday, and K. M. Górska, *Astrophys. J.* **644**, 701 (2006), astro-ph/0512433.
- [14] K. T. Inoue and J. Silk, *Astrophys. J.* **648**, 23 (2006), astro-ph/0602478.
- [15] L. R. Abramo, L. J. Sodré, and C. A. Wuensche, *Phys. Rev. D* **74**, 083515 (2006), astro-ph/0605269.
- [16] R. C. Helling, P. Schupp, and T. Tesileanu, *Phys. Rev. D* **74**, 063004 (2006), astro-ph/0603594.
- [17] J. G. Cresswell, A. R. Liddle, P. Mukherjee, and A. Riazuelo, *Phys. Rev. D* **73**, 041302 (2006), astro-ph/0512017.
- [18] H. K. Eriksen, A. J. Banday, K. M. Górska, and P. B. Lilje, *Astrophys. J.* **612**, 633 (2004), astro-ph/0403098.
- [19] G. Hinshaw *et al.*, *Astrophys. J. Lett.* **464**, L25 (1996).
- [20] M. Lachièze-Rey and J. Luminet, *Physics Report* **254**, 135 (1995).
- [21] J. Levin, *Physics Report* **365**, 251 (2002).
- [22] J. Luminet, J. R. Weeks, A. Riazuelo, R. Lehoucq, and J. Uzan, *Nature* **425**, 593 (2003).
- [23] R. Aurich, S. Lustig, and F. Steiner, *Class. Quantum Grav.* **22**, 2061 (2005), astro-ph/0412569.
- [24] R. Aurich, S. Lustig, and F. Steiner, *Class. Quantum Grav.* **22**, 3443 (2005), astro-ph/0504656.
- [25] J.-P. Uzan, A. Riazuelo, R. Lehoucq, and J. Weeks, *Phys. Rev. D* **69**, 043003 (2004), astro-ph/0303580.
- [26] R. Aurich, S. Lustig, F. Steiner, and H. Then, *Class. Quantum Grav.* **21**, 4901 (2004), astro-ph/0403597.
- [27] R. Aurich, S. Lustig, F. Steiner, and H. Then, *Phys. Rev. Lett.* **94**, 021301 (2005), astro-ph/0412407.
- [28] A. de Oliveira-Costa and M. Tegmark, *Phys. Rev. D* **74**, 023005 (2006), astro-ph/0603369.
- [29] W. Hu, *Wandering in the Background: A CMB Explorer*, PhD thesis, University of California at Berkeley, 1995, astro-ph/9508126.
- [30] C. J. Copi, D. Huterer, D. J. Schwarz, and G. D. Starkman, (2006), astro-ph/0605135.
- [31] J. Weeks and J. Gudermann, astro-ph/0611640 (2006).